



# HHS Public Access

Author manuscript

*J Magn Reson.* Author manuscript; available in PMC 2016 April 01.

Published in final edited form as:

*J Magn Reson.* 2015 April ; 253: 143–153. doi:10.1016/j.jmr.2015.01.001.

## Multiple Acquisition of Magic Angle Spinning Solid-State NMR Experiments Using One Receiver: Application to Microcrystalline and Membrane Protein Preparations

T. Gopinath<sup>1</sup> and Gianluigi Veglia<sup>1,2,\*</sup>

<sup>1</sup>Department of Biochemistry, Molecular Biology, and Biophysics, University of Minnesota, Minneapolis, MN 55455

<sup>2</sup>Department of Chemistry, University of Minnesota, Minneapolis, MN 55455

### Abstract

Solid-State NMR spectroscopy of proteins is a notoriously low-throughput technique. Relatively low-sensitivity and poor resolution of protein samples require long acquisition times for multidimensional NMR experiments. To speed up data acquisition, we developed a family of experiments called Polarization Optimized Experiments (POE), in which we utilized the orphan spin operators that are discarded in classical multidimensional NMR experiments, recovering them to allow simultaneous acquisition of multiple 2D and 3D experiments, all while using conventional probes with spectrometers equipped with one receiver. POEs allow the concatenation of multiple 2D or 3D pulse sequences into a single experiment, thus potentially combining all of the aforementioned advances, boosting the capability of ssNMR spectrometers at least two-fold without the addition of any hardware. In this Perspective, we describe the first generation of POEs, such as dual acquisition MAS (or DUMAS) methods, and then illustrate the evolution of these experiments into MEIOSIS, a method that enables the simultaneous acquisition of multiple 2D and 3D spectra. Using these new pulse schemes for the solid-state NMR investigation of biopolymers makes it possible to obtain sequential resonance assignments, as well as distance restraints, in about half the experimental time. While designed for acquisition of heteronuclei, these new experiments can be easily implemented for proton detection and coupled with other recent advancements, such as dynamic polarization, to improve signal to noise. Finally, we illustrate the application of these methods to microcrystalline protein preparations as well as single and multi-span membrane proteins reconstituted in lipid membranes.

---

© 2015 Published by Elsevier Inc.

\*To whom correspondence should be addressed: Gianluigi Veglia, Department of Biochemistry, Biophysics, and Molecular Biology, University of Minnesota, 6-155 Jackson Hall, MN 55455. Telephone: (612) 625-0758. Fax:(612) 625-2163. vegli001@umn.edu.

**Publisher's Disclaimer:** This is a PDF file of an unedited manuscript that has been accepted for publication. As a service to our customers we are providing this early version of the manuscript. The manuscript will undergo copyediting, typesetting, and review of the resulting proof before it is published in its final citable form. Please note that during the production process errors may be discovered which could affect the content, and all legal disclaimers that apply to the journal pertain.

## 1. Introduction

Magic angle spinning solid-state NMR (MAS ssNMR) spectroscopy is emerging as a unique method for the atomic resolution structure determination of biomacromolecules, such as membrane proteins and fibrils that are recalcitrant to crystallization. Recent reviews have illustrated the most important achievements in this field [1-3]. The advancements of this spectroscopy are due to the concomitant developments in high-field magnet technology, advances in probe design, isotopic-labeling schemes, and sample preparations, as well as pulse sequence design. However, sensitivity and resolution of the ssNMR spectra still limit the routine application of these techniques, particularly for membrane proteins, where lipids are used in the preparations to maintain the native conditions of the proteins.

There is no doubt that ssNMR structure determination of biomacromolecules is time consuming. Many hours or several days of signal averaging are required for a series of multidimensional experiments. In the classical experiments used for membrane proteins, low gyromagnetic ratio nuclei  $^{13}\text{C}$  and  $^{15}\text{N}$  are acquired, which are intrinsically insensitive. In the past few years, several approaches have been introduced to speed-up ssMAS NMR experiments, including dynamic nuclear polarization (DNP) at ultra-low temperatures[4-6], paramagnetic relaxation enhancement (PRE)[7-9], and  $^1\text{H}$  detection using ultra-fast MAS probes with or without perdeuteration [10, 11]. However, all these methods rely on sample modifications such as doping the samples with chemical compounds with unpaired electrons, use of low temperatures, and ultra-fast spinning speeds. While these methods have been successfully used for crystalline proteins, their application to membrane proteins is limited. To maintain their tertiary fold and function, membrane proteins need to be reconstituted in lipid membranes in a liquid crystalline phase[12, 13]. Lipid types as well as lipid to protein ratio are crucial parameters to maintain their functional integrity[12, 13]. Also, high spinning speeds can in several cases limit the application of ssMAS techniques[14]. For instance, enzyme function can be significantly reduced in the case of high spinning rates, although moderate spinning speeds can still be used to analyze the structural features of these enzymes.

In recent years, our group has been revisiting the classical NMR experiments for resonance assignment and distance determination in biological solids. Inspired by the previous work of Pines and Waugh [15], we asked ourselves: how much of the polarization generated by the experiments is actually converted into observable signals? Can we optimize the pulse sequences by recovering the *orphan spin operators* that are neglected or purged by the current pulse schemes?

Toward this goal, we developed a class of new experiments called Polarization Optimized Experiments (POE) that utilize orphan spin operators to generate multiple NMR spectra from one pulse sequence[16-19]. These experiments are carried out using commercial solid-state NMR probes for bio-solids and require only one receiver. To accomplish this task, we worked on the three main building blocks of the pulse sequences, including creation of the polarization, evolution, and detection. To generate extra operators to be utilized during the experiments, we introduced simultaneous cross polarization (SIM-CP)[18], generating multiple spin operators to be utilized in the generation of additional experiments. We

introduced the concept of bidirectional specific cross polarization[17], and the use of long-living  $^{15}\text{N}$  z-polarization[20] to generate parallel pathways of spin operators to detect several (up to four) multidimensional spectra[17], with at least two-fold time saving.

In this Perspective, we describe the most common experiments, such as dual acquisition MAS (DUMAS)[18, 19] and MEIOSIS (Multiple Experiments via Orphan Spin operatorS) [17], that enable the recording of three to four multi-dimensional experiments, explaining the principles and the technical details for concatenating multiple experiments together. We also project the use of these experiments in conjunction with other techniques, including  $^1\text{H}$  detection experiments. In the following synopsis, we will illustrate the optimization of the various steps and the implementations that make possible the simultaneous acquisition of multiple 2D, 3D, and 4D spectra.

## 2. Simultaneous cross-polarization

A central element in an MAS ssNMR experiment is the Hartmann-Hahn (HH) cross-polarization (CP)[21], which enables the polarization transfer from high ( $^1\text{H}$ ) to low gyromagnetic ratio nuclei ( $^{13}\text{C}$  or  $^{15}\text{N}$ ) (Figure 1A). The optimization of this first step is crucial for enhancing the sensitivity of the ssNMR experiments. For the POE experiments such as DUMAS and MEIOSIS, we create the initial polarization using a SIM-CP on three different channels. This scheme makes it possible to create both  $^{13}\text{C}$  and  $^{15}\text{N}$  polarization by satisfying the Hahn-Hartmann conditions for  $^1\text{H}$  and  $^{13}\text{C}$  as well as  $^1\text{H}$  and  $^{15}\text{N}$  (Figure 1B). The rotating frame radio frequency (RF) amplitudes for SIM-CP transfer are given by  $\omega_1 \pm n\omega_r$ ,  $\omega_1, \omega_1$  for  $^1\text{H}$ ,  $^{13}\text{C}$ , and  $^{15}\text{N}$ , respectively, where  $\omega_1$  is  $^{13}\text{C}$  and  $^{15}\text{N}$  RF amplitudes,  $\omega_r$  is MAS spinning frequency, and  $n$  is set to  $\pm 1$  or  $\pm 2$  to satisfy first or second sideband matching conditions, respectively. To test the efficiency of polarization transfer during SIM-CP, we performed a series of experiments on microcrystalline protein preparations or membrane proteins, varying spinning speeds and RF amplitudes. The  $^{13}\text{C}$  and  $^{15}\text{N}$  spectra are acquired separately using a single receiver. Importantly, we found that the  $^{13}\text{C}$  sensitivity is almost identical for CP and SIM-CP, whereas for  $^{15}\text{N}$  we observed  $\sim 5$ -10% loss. Moreover, the HH matching conditions for SIM-CP are identical to those of conventional CP. Therefore, the experimental setup for the SIM-CP is relatively straightforward. As an example, we report a comparison of CP and SIM-CP optimization profiles carried out with U- $^{13}\text{C}$ ,  $^{15}\text{N}$  ubiquitin (Figures 1C-D). The data points indicate the normalized integrated intensities of  $^{13}\text{C}$  and  $^{15}\text{N}$  at a spinning rate of 12 kHz. Notably, the build-up rates of the polarization transfer for both CP and SIM-CP are very similar, with SIM-CP showing only marginal loss (less than 10%) of sensitivity for  $^{15}\text{N}$  spectra with respect to conventional CP.

## 3. Bidirectional Specific-CP and Residual Polarization

In the conventional ssNMR pulse sequences for resonance assignments,  $^1\text{H}$ - $^{13}\text{C}$  or  $^1\text{H}$ - $^{15}\text{N}$  double resonance CP creates the initial  $^{13}\text{C}$  or  $^{15}\text{N}$  polarization, respectively. Thereafter, a specific-CP scheme[22] transfers the polarization between  $^{15}\text{N}$  and  $^{13}\text{C}$  from N to CA or CA to N in a unidirectional manner. We discovered that, using SIM-CP followed by specific-CP, it is possible to obtain a bidirectional polarization transfer between  $^{13}\text{C}$  (either CA or

CO) and  $^{15}\text{N}$ . This additional polarization can be detected using the sequence shown in Figure 2A, in which, after SIM-CP, the polarization is transferred from N to CA and, simultaneously, from CA to N. The CA polarization is detected in the first acquisition (blue FID); while the  $^{15}\text{N}$  polarization is stored along z-direction and then transferred to  $^{13}\text{CO}$  for a second acquisition (red FID). Figure 2B shows the two spectra obtained for U- $^{13}\text{C}$ ,  $^{15}\text{N}$  ubiquitin using the dual acquisition pulse sequence reported in Figure 2A, which utilizes SIM-CP and the bidirectional specific-CP for NCA and CAN transfers.

Similarly, it is possible to achieve bidirectional NCO and CON transfers using NCO specific-CP prior to first acquisition. In fact, the  $^{15}\text{N}$  polarization from a CON transfer can be stored during first acquisition and subsequently transferred to CA for a second acquisition time. For the optimization of the N-C specific-CP experiments, we utilize the 1D pulse sequences reported in Figure 2A. These sequences are used as building blocks for the 3D DUMAS experiments [19] that we will describe below. To cancel the residual polarization of  $^{13}\text{C}$  and  $^{15}\text{N}$ , we implemented a specific-CP sequence with a four-step phase cycle on  $^{13}\text{C}$  and  $^{15}\text{N}$  spin-lock pulse phases (see  $\varphi_2$  and  $\varphi_3$  in Figure 2A). Later on, we found that the residual polarization of  $^{13}\text{C}$  and  $^{15}\text{N}$  along with bidirectional polarization transfer creates *four* different polarization transfer pathways. These new coherences can also be detected and utilized to generate additional 2D and 3D experiments. This represented the genesis of MEIOSIS, a pulse scheme that enables one to detect four FIDs simultaneously. The one-dimensional experiment is shown in Figure 3A. Although conceptually similar to the experiment depicted in Figure 2A, the MEIOSIS pulse sequence has phase  $\varphi_2$  of the specific-CP set to x and  $\varphi_3$  switched between x and  $-x$ . This phase scheme enables one to decode the polarization into four data sets that are then stored into separate files representing four different polarization pathways: NCA, NN, CAN, and CC, where NCA and CAN refer to polarization transfer from N to CA and vice versa, and NN and CC refer to the residual magnetization on  $^{15}\text{N}$  and  $^{13}\text{C}$  that is not transferred to  $^{13}\text{C}$  and  $^{15}\text{N}$  during specific-CP. The first acquisition gives the  $^{13}\text{C}$  spectrum resulting from the NCA and CC pathways (Figure 3A). The  $^{15}\text{N}$  polarization resulting from the other two pathways (i.e., CAN and NN) is stored along the z direction, and at the end of the first acquisition, is transferred to  $^{13}\text{CO}$ . At this point, a second acquisition records the coherences resulting from the CAN and NN pathways. In order to decode the two pathways in each acquisition, we switch the specific-CP  $^{15}\text{N}$  spin-lock phase between  $+x$  and  $-x$  in alternate scans. The resultant time domain data for  $+x$  and  $-x$  phases are then separated prior to processing. Since the NCA and CAN transfers occur in a doubly tilted rotating frame, the phase switching of  $^{15}\text{N}$  spin-lock during specific-CP will invert the sign of the NCA and CAN transfer, whereas the residual CC or NN magnetization will not be affected by the phase switching. If the two data sets of the first acquisition with phases  $+x$  and  $-x$  are added, the CC transfer is summed, while the NCA transfer cancels out. On the other hand, if the two data sets are subtracted the NCA transfer is summed while the CC transfer cancels out, resulting into two different spectra. Similarly, the addition and subtraction of two data sets for the second acquisition will give magnetization resulting from NN and CAN pathways, respectively. Figure 3B shows the polarization build-up and decay of four pathways as a function of specific-CP contact period  $\tau$ , on U- $^{13}\text{C}$ ,  $^{15}\text{N}$  microcrystalline ubiquitin and a single-pass membrane protein, sarcolipin[16, 23-26]. At optimal polarization transfer ( $\sim 2800$  or  $3100 \mu\text{s}$ ) from N to CA

and vice versa, the residual polarization of  $^{13}\text{C}$  and  $^{15}\text{N}$  is approximately 55 and 35%, respectively.

#### 4. 2D DUMAS experiments

In the 2D DUMAS scheme, a  $^{13}\text{C}$ -edited experiment is concatenated with a  $^{15}\text{N}$ -edited experiment. Figure 4A shows a typical DUMAS pulse sequence where the  $^{13}\text{C}$ -edited CXCX experiment is combined with  $^{15}\text{N}$ -edited NCA experiment. The pulse sequence starts with SIM-CP to create an initial polarization for both  $^{13}\text{C}$  and  $^{15}\text{N}$  nuclei. In the first acquisition, the  $^{13}\text{C}$ -edited 2D experiment is recorded, while the  $^{15}\text{N}$  polarization is stored along the z-direction. The  $^{15}\text{N}$  polarization is then transferred to  $^{13}\text{C}$  and detected during the second acquisition giving the  $^{15}\text{N}$ -edited spectrum. As mentioned above, there are several different possibilities to combine  $^{13}\text{C}$ - and  $^{15}\text{N}$ -edited experiments using the DUMAS scheme. A non-comprehensive list of the most popular experiments is given in Figure 4C.

#### 5. On choosing the right combination of 2D DUMAS experiments

Although it is possible to concatenate several different experiments, it is critical to select  $^{13}\text{C}$  and  $^{15}\text{N}$ -edited experiments that maximize the sensitivity via dual acquisition. The  $^{13}\text{C}$ -edited experiments can be divided into two main categories. The first category includes the CXCX correlation experiments that make use of homonuclear polarization transfer among  $^{13}\text{C}$  nuclei. Typical experiments are DARR and PDSF, where shorter mixing periods (~15 to 30 ms) correlate intra-residue  $^{13}\text{C}$  chemical shifts, and longer mixing periods (~50 to 300 ms) correlate inter-residue  $^{13}\text{C}$  resonances at medium- and long-range distances. The second category is represented by selective homonuclear polarization transfer experiments such as CACB or CACO. These experiments use DREAM[27], SPC5[28], or R2TR mixing periods to correlate  $^{13}\text{C}$  resonances[29]. The  $^{15}\text{N}$ -edited experiments use NC specific-CP sequence for heteronuclear polarization transfer from  $^{15}\text{N}$  nuclei to CA or CO, giving NCA or NCO, respectively. Usually, the NC transfer is followed by CACX, COCX, CACB, or CACO mixing periods to obtain the classical 2D NCACX, NCOCX, NCACB, or NCACO experiments [30]. One has to consider that the relative sensitivity for these experiments depends on the nature and length of heteronuclear or homonuclear mixing periods as well as  $T_{1\rho}$  and  $T_2$  relaxation times. Notably, these features are quite different for membrane proteins and microcrystalline proteins. Although it is not possible to accurately predict the relative sensitivity of these multidimensional experiments based only on the 1D spectrum, one can roughly estimate the relative sensitivity from the 1<sup>st</sup> increment of the DUMAS experiments and follow the guidelines suggested by Wagner and co-workers[31]. Also, a major advantage of this method is that the building-block architecture of the DUMAS experiments make it possible to rearrange the pulse sequence and change the  $^{15}\text{N}$ -edited experiment to a different one, while continuing acquiring the  $^{13}\text{C}$ -edited experiment in the first acquisition.

As a case study, consider the combination of CXCX with NCA and NCO experiments. In general, NCA and NCO experiments are relatively shorter than the CXCX experiments, which require 20-40 ms of mixing periods. Therefore, it is convenient to set the 2D DUMAS experiments to acquire the CXCX experiment in the first part of the pulse sequence (i.e.,

first acquisition period) with  $n$  scans, and the NCA and NCO experiments in the second part of the pulse sequence (i.e., second acquisition) with  $n/2$  scans for each experiments. In other words, two pulse programs are encoded with CXCX-NCA and CXCX-NCO combinations, with identical CXCX block followed by NCA and NCO, respectively. The resulting data sets (the first for CXCX-NCA, and the second for CXCX-NCO) are stored in separate memory locations. The CXCX acquisitions are added prior to processing, whereas the NCA and NCO spectra are processed separately.

Another important aspect is the optimization of the  $t_1$  evolution parameters. While the  $t_2$  acquisition parameters are identical for both acquisitions, the  $t_1$  evolution parameters need to be optimized. In a typical  $^{13}\text{C}$ -edited experiment, a full  $^{13}\text{C}$  spectral width of 180 ppm is used in the indirect dimension. On the other hand,  $^{15}\text{N}$ -edited experiments require only about one tenth of the  $^{13}\text{C}$  spectral width or ten times the  $^{13}\text{C}$  dwell time ( $t_1$ ). Since the  $t_1$  evolution periods of  $^{13}\text{C}$  and  $^{15}\text{N}$  dimensions are coded separately for the 2D DUMAS pulse sequence, it is possible to choose two different dwell times and numbers of increments for  $^{13}\text{C}$  and  $^{15}\text{N}$  while satisfying the maximum  $t_1$  evolution time and number of scans as shown in table 1. The integer 'C' dictates the dwell time and maximum  $t_1$  evolution time for an  $^{15}\text{N}$ -edited experiment. Of course, depending on the desired spectral width, it is possible to choose other combinations of  $^{13}\text{C}$  and  $^{15}\text{N}$  dwell times by adjusting the 'C' value. The value of 'C' ranges from 3 to 10, depending on the ratio of  $^{13}\text{C}$  and  $^{15}\text{N}$  increments (see Table 1). Figure 4D shows the simultaneous acquisition of 2D CXCX-NCA DUMAS experiments on a U- $^{13}\text{C}$ ,  $^{15}\text{N}$ -labeled membrane protein, phospholamban.

## 6. One experiment gives four spectra: MEIOSIS

Several multidimensional  $^{13}\text{C}$ -edited experiments, including CA(N)CO, CO(N)CA, CA(N)COCX, and CO(N)CACX, make use of two heteronuclear (NC) polarization transfer steps with or without CC mixing sequence. In these experiments, the first NC transfer step corresponds to NCA and second NCO (or vice-versa). We will refer to them as CNC- or CNCC-type experiments[32]. These experiments detect the inter-residue correlations between CA and CO resonances and are used as a complement to the CXCX-type of experiments, though they are less sensitive due to the double NC transfer steps. Nonetheless, unlike CXCX experiments they offer unambiguous one-to-one correlations for assigning the backbone of medium-sized proteins. Using similar principles to the DUMAS experiments, we developed new pulse sequences that combine one CNCC, one CC, and two  $^{15}\text{N}$ -edited experiments. Referencing the biological concept of meiosis, we called these experiments MEIOSIS. In fact, by combining bidirectional polarization transfer with residual polarization, we were able to create four polarization pathways that are then used for recording four different 2D experiments. Figure 5A shows the general scheme for the 2D MEIOSIS experiments. Briefly, the pulse sequence starts with SIM-CP to create initial  $^{13}\text{C}$ - and  $^{15}\text{N}$ - polarization, followed by a  $t_1$  evolution period. During the subsequent NC transfer, four polarization pathways are created, namely CC, NC, NN, and CN pathways. The residual  $^{13}\text{C}$  and  $^{15}\text{N}$  polarization results from CC and NN transitions, whereas NC and CN are the transferred polarization from  $^{15}\text{N}$  to  $^{13}\text{C}$  (CA or CO) and vice versa. At this point, the  $^{13}\text{C}$  polarization resulting from CC and NC pathways undergoes homonuclear polarization transfer during a CC mixing period, followed by  $t_2$  acquisition, while the  $^{15}\text{N}$

polarization from the NN and CN pathways is stored along the z direction. Based on the mixing sequence, the first acquisition can give either CXCX and NCC or CACB and NCACB spectra. After the first acquisition,  $^{15}\text{N}$  polarization from NN and CN pathways is transferred to  $^{13}\text{C}$ , followed by homonuclear CC mixing and the acquisition time ( $t_2$ ), at the same time the NN and CN pathways generated are converted into the NCC and CNCC spectra, respectively. We have analyzed both the residual and transferred polarizations of NCA and NCO resulting from the specific-CP for microcrystalline as well as membrane proteins. At optimal NCA or CAN specific-CP mixing time, we detected approximately 50-55% residual  $^{13}\text{C}$  polarization and 30-35%  $^{15}\text{N}$  polarization (Figure 3).

As for the DUMAS experiments, it is important to select and concatenate the appropriate pulse sequences to yield the highest possible sensitivity. In fact, the choice of the CNCC experiment will dictate the possible combinations of the three other experiments. In the typical MEIOSIS scheme, the first and second specific-CP transfers are set to NCA and NCO, or vice versa, whereas the first and second mixing periods are set for CXCX or CACB homonuclear transfer. By permuting these NC and CC mixing periods, it is possible to obtain multiple combinations of these experiments (Figure 5B). For example, the CA(N)CO experiment can be combined with CXCX, NCACX, and NCO, with CXCX and NCACX acquired during the first acquisition period and the CA(N)CO and NCO experiments during the second acquisition period. The latter is accomplished by setting the second mixing period in the pulse sequence to zero. Note that the spectra resulting from the second acquisition are relatively insensitive with respect to those from the first acquisition period. To optimize the acquisition of CACB or CXCX spectra, we usually set the second mixing time to zero. Alternatively, longer mixing periods ( $\sim 100$ - $200$  ms) prior to the first acquisition and shorter mixing periods ( $\sim 20$  to  $40$  ms) during the second acquisition can be used to obtain comparable sensitivity for both acquisitions.

Unlike the DUMAS schemes, the  $t_1$  evolution periods in the MEIOSIS experiments for the two  $^{13}\text{C}$ -edited experiments and the corresponding  $^{15}\text{N}$ -edited experiments are time-shared. Although CNC experiments require a smaller spectral width in the indirect dimension (i.e., approximately 30-40 ppm), the dwell time ( $t_1'$ ) is set to cover approximately 185 ppm. The latter makes the spectral width in the indirect dimension compatible with the acquisition of a CC-type experiment. As for the 2D DUMAS,  $^{15}\text{N}$  evolution time ( $t_1''$ ) and the effective number of scans are chosen according to Table 1. Figure 5C shows the simultaneous acquisition of CXCX, NCACX, CA(N)CO and NCO 2D spectra on U- $^{13}\text{C}$ ,  $^{15}\text{N}$  labeled microcrystalline ubiquitin.

## 7. 3D DUMAS experiments

The  $^{13}\text{C}$ -detected 3D ssNMR experiments can be divided into two main categories: A)  $^{13}\text{C}$ - and  $^{15}\text{N}$ -edited (CNC or CNCC), and B)  $^{15}\text{N}$ - and  $^{13}\text{C}$ -edited (NCC) experiments, which start with a  $^1\text{H}$ - $^{13}\text{C}$  and  $^1\text{H}$ - $^{15}\text{N}$  double resonance cross polarization sequence[33]. After the initial CP, these pulse sequences comprise two heteronuclear and homonuclear polarization transfer periods sandwiched between two evolution periods ( $t_1$  and  $t_2$ ) followed by the acquisition period for the third dimension ( $t_3$ ). Several of these 3D experiments can be concatenated into one multiple spectra-generating experiment using the DUMAS approach.

A typical 3D DUMAS experiment (Figure 6A) starts with SIM-CP to create the initial  $^{13}\text{C}$  and  $^{15}\text{N}$  polarization that can be exploited to obtain NCC and CNC (or CNCC) experiments simultaneously. The NCC experiment is recorded in the first acquisition period, whereas the CNC experiment is recorded in the second. Specific-CP is used for heteronuclear transfer between  $^{15}\text{N}$  and  $^{13}\text{CA}$  (or  $^{13}\text{CO}$ ), whereas CC (or alternatively CACB or CACO) homonuclear transfer is obtained using mixing sequences such as DREAM, SPC5, and R2TR. Both NCC and CNC polarization pathways originate from the same NC or CN specific-CP period via a bidirectional transfer followed by a  $t_1$  evolution period. The NCC experiment, which is preceded by a  $t_2$  evolution period and  $^{13}\text{C}$  homonuclear mixing, is recorded during the first acquisition period ( $t_3'$ ), while the  $^{15}\text{N}$  polarization is stored along the z-direction. After the first acquisition, a  $90^\circ$  degree pulse brings the  $^{15}\text{N}$  polarization in the transverse plane, which is then allowed to evolve under during an evolution period  $t_2$ . An NC specific-CP transfers the polarization from  $^{15}\text{N}$  to CA/CO and, after a mixing period, the CNC experiment is acquired during the  $t_3$  period. Alternatively, the homonuclear mixing can be applied prior to the second acquisition period to obtain a CNCC experiment. The first and second specific-CP sequences are optimized for NCA and NCO transfer, giving  $^{15}\text{N}$ -,  $^{13}\text{Ca}$ -edited and  $^{13}\text{Ca}$ -,  $^{15}\text{N}$ -edited experiments in the first and second acquisitions, respectively. Sometimes, however, it is advantageous to evolve  $^{13}\text{CO}$  in the indirect evolution periods. In this case, it is possible to obtain  $^{13}\text{CO}$ -edited DUMAS experiments by switching the specific-CP periods. During the mixing period, the non-selective CXCX transfer is obtained via DARR [34] or PDS [35] sequences, whereas the selective CACB (or CACO) transfer is achieved using DREAM or R2TR sequences. The  $t_1$  and  $t_2$  dwell times for  $^{13}\text{Ca}$  ( $^{13}\text{CO}$ ) and  $^{15}\text{N}$  are set to cover the required spectral widths. Typically the dwell time for  $^{13}\text{Ca}$  is set to 0.5 to 0.7 times that of  $^{15}\text{N}$ , whereas the dwell time for  $^{13}\text{CO}$  is set equal to that of  $^{15}\text{N}$ . Depending on the type and length of CC mixing period, several pairs of NCC and CNCC experiments can be combined in the 3D DUMAS experiments. For instance, NCACX or NCACB can be combined with CANCO or CAN(CO)CX experiments. Similarly, NCOCX can be combined with CONCA, CONCACX, or CONCACB. For CACB or CACO selective transfers, mixing times of 5 to 10 ms are generally used. In contrast, for non-selective CACX or COCX transfers, several mixing times are used to obtain sequential, medium, and long-range correlations. While longer mixing times result in more correlations in the spectra, they also lower the overall sensitivity of the experiment. Additionally, the presence of two specific-CP periods for the CNCC experiment lowers its sensitivity by about 30-50% as compared to the NCC experiment. For this reason, we usually run this experiment without, or with a very short, mixing period prior to the second acquisition. In the absence of a mixing period, the second acquisition gives CANCO or CONCA, whereas the incorporation a CC mixing period yields CANCOCX or CONCACX. Figure 6c shows an example of simultaneous acquisition of NCACX and CANCO on a U- $^{13}\text{C}$ ,  $^{15}\text{N}$  microcrystalline ubiquitin sample.

## 8. 3D Meiosis

The combination of residual and transferred polarization of specific-CP can be used for acquiring multiple three-dimensional experiments [17]. The general protocol of 3D MEIOSIS is shown in Figure 7. The 3D experiments originate from the 2D MEIOSIS pulse

sequence (Figure 5A), with the addition of an evolution period ( $t_2'$  and  $t_2''$ ) prior to the mixing periods. The pulse sequence starts with SIM-CP to create the initial  $^{13}\text{C}$  and  $^{15}\text{N}$  polarization, which is then evolved during the  $t_1'$  and  $t_1''$  evolution periods, then followed by an NC/CN specific-CP transfer. The NC/CN transfer creates four polarization pathways, including bidirectional transfer from N to C (CA or CO) and C to N, as well as residual polarization (CC and NN pathways) of  $^{13}\text{C}$  and  $^{15}\text{N}$  nuclei. The  $^{15}\text{N}$  polarization resulting from the NN and CN pathways is stored along the z-direction; whereas the  $^{13}\text{C}$  polarization from NC and CC pathways is evolved during  $t_2$ , followed by a mixing period and the  $t_3'$  acquisition period, which corresponds to the sum of the NCC and CCC 3D experiments, respectively. After the first acquisition, the  $^{15}\text{N}$  polarization is transferred to CO or CA, then evolved during  $t_2$  followed by the mixing period and  $t_3''$  acquisition. This second acquisition is the sum of two 3D experiments, C(N)CC and NCC, resulting from the CN and NN pathways, respectively. As with the 2D MEIOSIS, two data sets are recorded with the  $^{15}\text{N}$  spinlock phase of the first specific-CP set to  $+x$  and  $-x$ , and stored in separate memory locations. The phase switching of the  $^{15}\text{N}$  spinlock will not affect the residual polarization, but it will invert the phase of the transferred polarization from the NC and CN pathways. The sum of these two data sets will give CCC and NCC experiments in the first and second acquisitions, respectively, cancelling out the NCC and CNCC coherences; whereas the difference of the two data sets will give NCC and C(N)CC experiments. The  $t_1$  and  $t_2$  evolution of the CCC experiment are identical, giving an aliased DARR spectrum along the F1-F2 diagonal; therefore, this data set is discarded. According to the scheme in Figure 6, the 3D MEIOSIS method combines a C(N)CC experiment with two  $^{15}\text{N}$ - and  $^{13}\text{C}$ -edited experiments for the simultaneous acquisition of three 3D experiments. As with the 2D MEIOSIS, the sensitivity of the C(N)CC and NCC experiments that are acquired during the second acquisition is lower compared to the NCC experiment recorded in the first acquisition. This is expected since the C(N)CC experiment requires two specific-CP periods, while the NCC experiment of the second acquisition utilizes the  $^{15}\text{N}$  residual polarization, which is typically 30-35% of the absolute intensity. However, the sensitivity of both acquisitions can be optimized by using different lengths of mixing periods as explained in the 2D MEIOSIS section. Depending on the choice of C(N)CC experiment, two other NCC experiments can be combined using 3D MEIOSIS method. For example CA(N)COCX is combined with NCACX and NCOCX, similarly CO(N)CACX is combined with NCOCX and NCACX. The 3D C(N)CC and NCC experiments resulting from the second acquisition are relatively insensitive compared to NCC experiment of the first acquisition. As for the 2D MEIOSIS, the sensitivity is optimized by choosing a longer (50 to 100 ms) and shorter (20 to 30 ms) mixing times prior to the first and second acquisitions, respectively. Similarly other two combinations of 3D MEIOSIS can be obtained by using selective CACB transfer prior to the first or second acquisition. Examples of 3D NCACX-CA(N)COCX-NCOCX MEIOSIS spectra are reported in Figure 7C.

## 9. Sequential assignment of soluble and membrane bound proteins using POEs

Sequential assignment of chemical shifts is the first step towards the structure determination of proteins. For a number of reasons, protein assignment concepts in solid-state NMR are

intrinsically different to those known from solution NMR triple resonance experiments involving  $^1\text{H}$  detection. Proton detection in solid-state NMR is still challenging, even with high-frequency MAS. Here we show the application of DUMAS and MEIOSIS based  $^{13}\text{C}$ -detected experiments for the assignment of uniformly  $^{13}\text{C}$ - and  $^{15}\text{N}$ -labeled ubiquitin and sarcolipin proteins. In both cases, sequential assignment was achieved by using a single experiment, namely DUMAS-NCACX-CANCO. While for ubiquitin 56 out of 76 residues were assigned, for sarcolipin the entire transmembrane region (22 out of 31 residues) was assigned (Figure 8).

## 10. Discussion

Rather than a suite of new pulse sequences, POE illustrates a novel approach to optimize the existing experiments using the classical setup of NMR spectrometers and acquire multiple 2D and 3D experiments, reducing by half the experimental time. In the most favorable cases, this approach enables spectroscopists to double the capacity of the spectrometer; while in other cases the additional spectra can be stored and summed later on with other acquisitions. The overall philosophy of the approach is to *make the best out of the polarization generated*. The existence of unused polarization that was not converted into observable coherences (orphan spin operators) was pointed out by Pines and Waugh [15]. Historically, the solution NMR community has been the most attentive to detect multiple spin operators for simultaneous acquisition of 2D experiments such as COSY-NOESY [36] and COCONOSY [37] and/or enhance the signal [38]. More recently, the *afterglow* phenomenon exploited by Kay and co-workers opened up the possibility for the acquisition of multidimensional NMR spectra of proteins in parallel [39]. The latter approach has been implemented with either one or multiple receivers [40-42]. Sensitivity enhanced experiments in solids have also been proposed by Tycko and co-workers [43] and been implemented in a manner similar to the sensitivity enhancement for solution NMR experiments. Moreover, Takegoshi and co-workers have implemented the equivalent of COCONOSY for solids [44] as well as the double acquisition using discarded coherences in 2D spectra with the States method [45], paving the way for multiple acquisition in biological solids.

For POE, the creation of two polarization transfer pathways via SIM-CP in which the relatively long-living  $^{15}\text{N}$  polarization allows one to acquire additional NMR experiments. Another important property we discovered is the bidirectional  $^{15}\text{N}$ - $^{13}\text{C}$  polarization transfer, which enables one to rescue the orphan spin operators resulting from residual polarization and obtain multiple 2D and 3D experiments to be detected simultaneously.

In the past few year, the POE family has expanded. It now includes the  $^1\text{H}$  detected experiments under fast MAS conditions [46], the afterglow sequence developed by Traaseth and coworkers [47, 48], the simultaneous acquisition of PAIN and PAR experiments discovered by Meier and coworkers [49] as well as the more recent pulse sequences that are the dipolar-edited versions of DUMAS methodology [50]. These experiments reinforce the importance of developing pulse sequences that exploit as many orphan operators as possible to enhance the NMR signal in solids and enable multiple acquisitions.

## 11. Conclusions and Perspectives

Sensitivity and resolution are the two *devils* that pester NMR spectroscopy. However, we believe that there is a lot of room for new developments in solid-state NMR of biomacromolecules. While we (as researchers) have the tendency to reassure our audience that *all of the methods are in place*, in actuality, there are plenty of improvements that must be done to make this technique flourish. It is hard to predict whether the current methods will survive the rapid progress of many groups in this field. Our contribution, however, underscores the fact that even the most robust experiments used for the routine resonance assignment of biopolymers can be improved. The techniques that we reviewed in this paper can be implemented in commercially available spectrometers without additional hardware. Commercial probes for biomacromolecules can be utilized with only a single receiver, effectively doubling the capacity of the spectrometer. Given the long-living nature of  $^{15}\text{N}$  polarization, we expect that several other groups will take on this approach, which in our opinion represents a totally new way to speed up solid-state NMR data acquisition. An obvious extension of this approach is inverse detection experiments, which will enable higher sensitivity and the possibility to recover even more orphan operators to give additional spectra. Another development includes the possibility of using double receivers, optimizing data collection and processing. Finally, our methods do not preclude other approaches to be implemented. In fact, when applied in concert with other fast acquisition and sensitivity enhancement techniques (e.g., Dynamic Nuclear Polarization and/or Paramagnetic Relaxation Enhancements), our methods will increase the throughput of high-resolution structure determination by MAS NMR.

## Acknowledgments

This work is supported by the National Institute of Health (GM 64742 and GM 72701). The NMR experiments were carried out at the Minnesota NMR Center.

## References

1. Hong M, Zhang Y, Hu F. Membrane protein structure and dynamics from NMR spectroscopy. *Annu Rev Phys Chem.* 2012; 63:1–24. [PubMed: 22136620]
2. McDermott A. Structure and Dynamics of Membrane Proteins by Magic Angle Spinning Solid-State NMR. *Annual review of biophysics.* 2009:385–403.
3. Baker LA, Baldus M. Characterization of membrane protein function by solid-state NMR spectroscopy. *Curr Opin Struct Biol.* 2014; 27C:48–55. [PubMed: 24865155]
4. Maly T, Debelouchina GT, Bajaj VS, Hu KN, Joo CG, Mak-Jurkauskas ML, Sirigiri JR, van der Wel PC, Herzfeld J, Temkin RJ, Griffin RG. Dynamic nuclear polarization at high magnetic fields. *J Chem Phys.* 2008; 128:052211. [PubMed: 18266416]
5. Rossini AJ, Zagdoun A, Lelli M, Lesage A, Coperet C, Emsley L. Dynamic nuclear polarization surface enhanced NMR spectroscopy. *Acc Chem Res.* 2013; 46:1942–1951. [PubMed: 23517009]
6. Sze KH, Wu Q, Tse HS, Zhu G. Dynamic nuclear polarization: new methodology and applications. *Topics in current chemistry.* 2012; 326:215–242. [PubMed: 22057860]
7. Wickramasinghe NP, Kotecha M, Samoson A, Past J, Ishii Y. Sensitivity enhancement in  $(^{13}\text{C})$  solid-state NMR of protein microcrystals by use of paramagnetic metal ions for optimizing  $(^1\text{H})$   $T(1)$  relaxation. *J Magn Reson.* 2007; 184:350–356. [PubMed: 17126048]
8. Parthasarathy S, Nishiyama Y, Ishii Y. Sensitivity and resolution enhanced solid-state NMR for paramagnetic systems and biomolecules under very fast magic angle spinning. *Acc Chem Res.* 2013; 46:2127–2135. [PubMed: 23889329]

9. Wickramasinghe NP, Parthasarathy S, Jones CR, Bhardwaj C, Long F, Kotecha M, Mehboob S, Fung LW, Past J, Samoson A, Ishii Y. Nanomole-scale protein solid-state NMR by breaking intrinsic IHT1 boundaries. *Nat Methods*. 2009; 6:215–218. [PubMed: 19198596]
10. Reif B. Ultra-high resolution in MAS solid-state NMR of perdeuterated proteins: implications for structure and dynamics. *J Magn Reson*. 2012; 216:1–12. [PubMed: 22280934]
11. Agarwal V, Penzel S, Szekely K, Cadalbert R, Testori E, Oss A, Past J, Samoson A, Ernst M, Bockmann A, Meier BH. De Novo 3D Structure Determination from Sub-milligram Protein Samples by Solid-State 100 kHz MAS NMR Spectroscopy. *Angewandte Chemie*. 2014
12. Murray DT, Li C, Gao FP, Qin H, Cross TA. Membrane protein structural validation by oriented sample solid-state NMR: diacylglycerol kinase. *Biophys J*. 2014; 106:1559–1569. [PubMed: 24739155]
13. Cross TA, Ekanayake V, Paulino J, Wright A. Solid state NMR: The essential technology for helical membrane protein structural characterization. *J Magn Reson*. 2014; 239:100–109. [PubMed: 24412099]
14. Miao Y, Cross TA. Solid state NMR and protein-protein interactions in membranes. *Curr Opin Struct Biol*. 2013
15. Pines A, Gibby MG, Waugh JS. Proton-enhanced NMR of dilute spins in solids. *J Chem Phys*. 1973; 59:569–590.
16. Mote KR, Gopinath T, Veglia G. Determination of structural topology of a membrane protein in lipid bilayers using polarization optimized experiments (POE) for static and MAS solid state NMR spectroscopy. *J Biomol NMR*. 2013; 57:91–102. [PubMed: 23963722]
17. Gopinath T, Veglia G. Orphan spin operators enable the acquisition of multiple 2D and 3D magic angle spinning solid-state NMR spectra. *J Chem Phys*. 2013; 138:184201. [PubMed: 23676036]
18. Gopinath T, Veglia G. Dual acquisition magic-angle spinning solid-state NMR-spectroscopy: simultaneous acquisition of multidimensional spectra of biomacromolecules. *Angewandte Chemie*. 2012; 51:2731–2735. [PubMed: 22311700]
19. Gopinath T, Veglia G. 3D DUMAS: simultaneous acquisition of three-dimensional magic angle spinning solid-state NMR experiments of proteins. *J Magn Reson*. 2012; 220:79–84. [PubMed: 22698806]
20. Giraud N, Bockmann A, Lesage A, Penin F, Blackledge M, Emsley L. Site-specific backbone dynamics from a crystalline protein by solid-state NMR spectroscopy. *J Am Chem Soc*. 2004; 126:11422–11423. [PubMed: 15366872]
21. Hartmann SR, Hahn EL. Nuclear Double Resonance in the Rotating Frame. *Physical Review*. 1962; 128:2042–2053.
22. Baldus M, Petkova AT, Herzfeld J, Griffin RG. Cross polarization in the tilted frame: assignment and spectral simplification in heteronuclear spin systems. *Molecular Physics*. 1998; 95:1197–1207.
23. Shi L, Cembran A, Gao J, Veglia G. Tilt and azimuthal angles of a transmembrane peptide: a comparison between molecular dynamics calculations and solid-state NMR data of sarcolipin in lipid membranes. *Biophys J*. 2009; 96:3648–3662. [PubMed: 19413970]
24. Mascioni A, Karim C, Barany G, Thomas DD, Veglia G. Structure and orientation of sarcolipin in lipid environments. *Biochemistry*. 2002; 41
25. Traaseth NJ, Ha KN, Verardi R, Shi L, Buffy JJ, Masterson LR, Veglia G. Structural and dynamic basis of phospholamban and sarcolipin inhibition of Ca(2+)-ATPase. *Biochemistry*. 2008; 47:3–13. [PubMed: 18081313]
26. Buffy JJ, Traaseth NJ, Mascioni A, Gor'kov PL, Chekmenev EY, Brey WW, Veglia G. Two-dimensional solid-state NMR reveals two topologies of sarcolipin in oriented lipid bilayers. *Biochemistry*. 2006; 45:10939–10946. [PubMed: 16953579]
27. Verel R, Ernst M, Meier BH. Adiabatic dipolar recoupling in solid-state NMR: the DREAM scheme. *J Magn Reson*. 2001; 150:81–99. [PubMed: 11330986]
28. Hohwy M, Rienstra CM, Jaroniec CP, Griffin RG. Fivefold symmetric homonuclear dipolar recoupling in rotating solids: Application to double quantum spectroscopy. *J Chem Phys*. 1999; 110:7983–7992.
29. Takegoshi K, Nomura K, Terao T. Rotational resonance in the tilted rotating frame. *Chem Phys Letters*. 1995; 232:424–428.

30. Pauli J, Baldus M, van Rossum B, de Groot H, Oschkinat H. Backbone and side-chain  $^{13}\text{C}$  and  $^{15}\text{N}$  signal assignments of the alpha-spectrin SH3 domain by magic angle spinning solid-state NMR at 17.6 Tesla. *Chembiochem*. 2001; 2:272–281. [PubMed: 11828455]
31. Rovnyak D, Hoch JC, Stern AS, Wagner G. Resolution and sensitivity of high field nuclear magnetic resonance spectroscopy. *Journal of Biomolecular Nmr*. 2004; 30:1–10. [PubMed: 15452430]
32. Franks WT, Kloepper KD, Wylie BJ, Rienstra CM. Four-dimensional heteronuclear correlation experiments for chemical shift assignment of solid proteins. *Journal of Biomolecular Nmr*. 2007; 39:107–131. [PubMed: 17687624]
33. Castellani F, van Rossum B, Diehl A, Schubert M, Rehbein K, Oschkinat H. Structure of a protein determined by solid-state magic-angle-spinning NMR spectroscopy. *Nature*. 2002; 420:98–102. [PubMed: 12422222]
34. Takegoshi K, Nakamura S, Terao T. C-13-H-1 dipolar-assisted rotational resonance in magic-angle spinning NMR. *Chemical Physics Letters*. 2001; 344:631–637.
35. Suter D, Ernst RR. Spin Diffusion in Resolved Solid-State NMR Spectra. *Phys Rev B*. 1985; 32:5608–5627.
36. Gurevich AZ, Barsukov IL, Arseniev AS, Bystrov VF. Combined COSY-NOESY Experiment. *J Magn Reson*. 1984; 56:471–478.
37. Haasnoot CAG, van de Ven FJM, Hilbers CW. COCONOSY. Combination of 2D Correlated and 2D Nuclear Overhauser Enhancement Spectroscopy in a Single Experiment. *J Magn Reson*. 1984; 56:343–349.
38. Kay LE, Keifer P, Saarinen T. Pure Absorption Gradient Enhanced Heteronuclear Single Quantum Correlation Spectroscopy with Improved Sensitivity. *J Am Chem Soc*. 1992; 114:10663–10665.
39. Kupce E, Kay LE, Freeman R. Detecting the “afterglow” of  $^{13}\text{C}$  NMR in proteins using multiple receivers. *J Am Chem Soc*. 2010; 132:18008–18011. [PubMed: 21126087]
40. Wiedemann C, Bellstedt P, Herbst C, Gorlach M, Ramachandran R. An approach to sequential NMR assignments of proteins: application to chemical shift restraint-based structure prediction. *J Biomol NMR*. 2014; 59:211–217. [PubMed: 24943494]
41. Kupce E, Kay LE. Parallel acquisition of multi-dimensional spectra in protein NMR. *J Biomol NMR*. 2012; 54:1–7. [PubMed: 22802131]
42. Chakraborty S, Paul S, Hosur RV. Simultaneous acquisition of  $^{13}\text{C}$ alpha- $^{15}\text{N}$  and  $^1\text{H}$ - $^{15}\text{N}$ - $^{15}\text{N}$  sequential correlations in proteins: application of dual receivers in 3D HNN. *J Biomol NMR*. 2012; 52:5–10. [PubMed: 22203187]
43. Tycko R. Sensitivity enhancement in two-dimensional solid-state NMR spectroscopy by transverse mixing. *Chemphyschem*. 2004; 5:863–868. [PubMed: 15253312]
44. Fukuchi M, Takegoshi K. Combination of  $(^{13}\text{C})\text{-}(^{13}\text{C})$  COSY and DARR (COCODARR) in solid-state NMR. *Solid State Nucl Magn Reson*. 2008; 34:151–153. [PubMed: 18635343]
45. Fukuchi M, Inukai M, Takeda K, Takegoshi K. Double-acquisition: utilization of discarded coherences in a 2D separation experiment using the States method. *J Magn Reson*. 2008; 194:300–302. [PubMed: 18667347]
46. Bellstedt P, Herbst C, Hafner S, Leppert J, Gorlach M, Ramachandran R. Solid state NMR of proteins at high MAS frequencies: symmetry-based mixing and simultaneous acquisition of chemical shift correlation spectra. *J Biomol NMR*. 2012; 54:325–335. [PubMed: 23180049]
47. Banigan JR, Gayen A, Traaseth NJ. Combination of  $(^1)^{(5)}\text{N}$  reverse labeling and afterglow spectroscopy for assigning membrane protein spectra by magic-angle-spinning solid-state NMR: application to the multidrug resistance protein EmrE. *J Biomol NMR*. 2013; 55:391–399. [PubMed: 23539118]
48. Banigan JR, Traaseth NJ. Utilizing afterglow magnetization from cross-polarization magic-angle-spinning solid-state NMR spectroscopy to obtain simultaneous heteronuclear multidimensional spectra. *The journal of physical chemistry B*. 2012; 116:7138–7144. [PubMed: 22582831]
49. Nielsen AB, Szekely K, Gath J, Ernst M, Nielsen NC, Meier BH. Simultaneous acquisition of PAR and PAIN spectra. *J Biomol NMR*. 2012; 52:283–288. [PubMed: 22371268]

50. Das BB, Opella SJ. Multiple acquisition/multiple observation separated local field/chemical shift correlation solid-state magic angle spinning NMR spectroscopy. *J Magn Reson.* 2014; 245:98–104. [PubMed: 25023566]

Author Manuscript

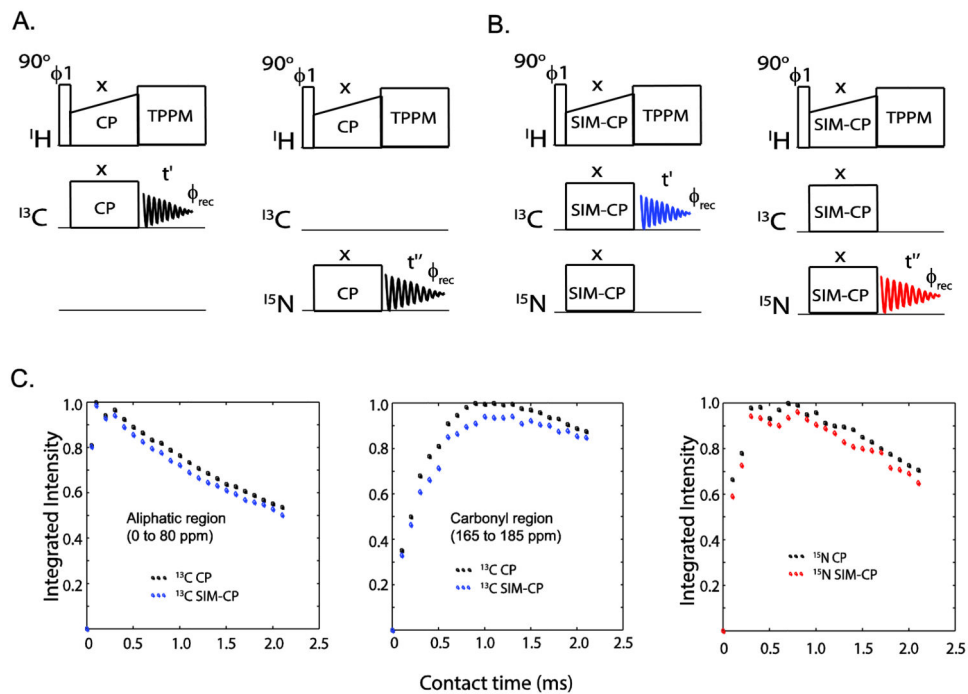
Author Manuscript

Author Manuscript

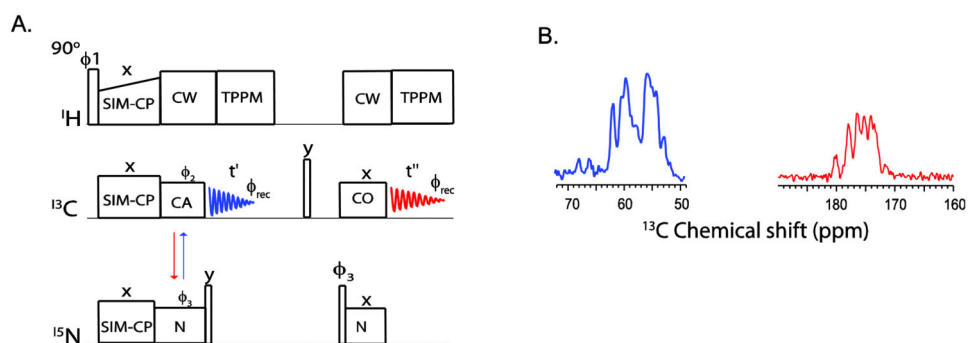
Author Manuscript

### Highlights

- Acquisition of multiple solid-state NMR experiments using only one receiver
- DUMAS enables the simultaneous acquisition of two MAS NMR spectra
- 3D DUMAS: acquisition of two 3D spectra simultaneously
- MEIOSIS make it possible to acquire four 2D spectra or three 3D spectra simultaneously

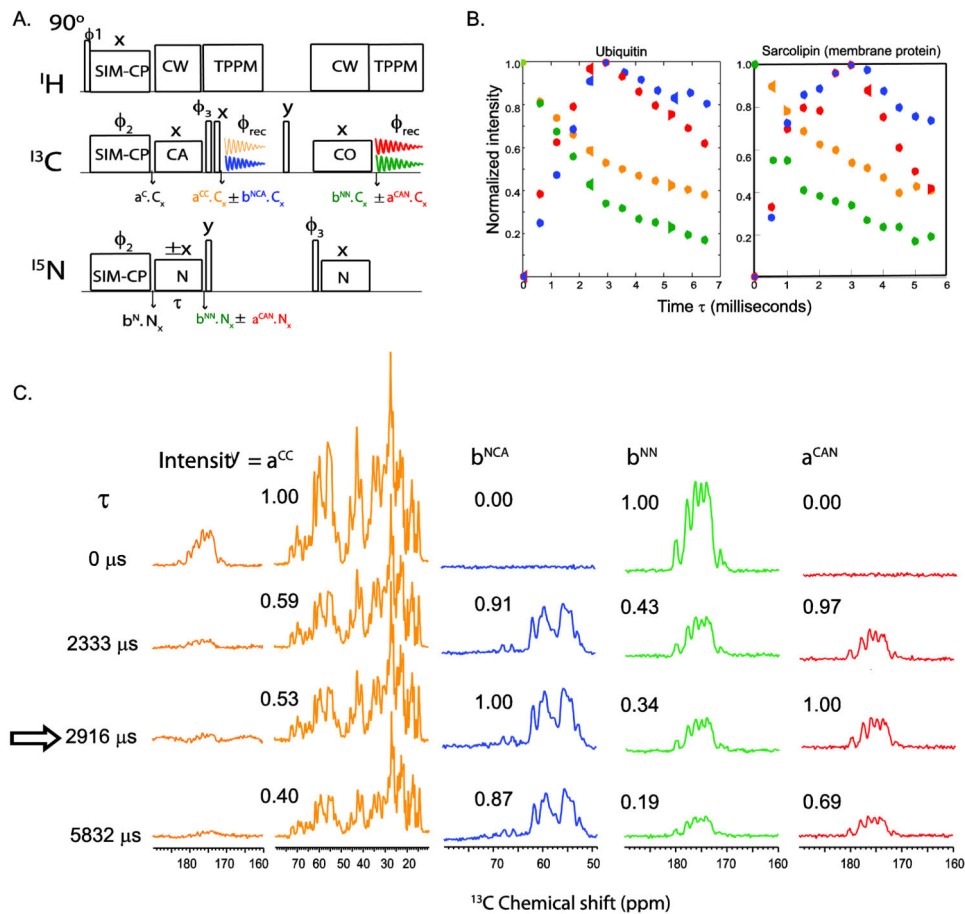


**Figure 1.** Pulse sequences utilized for the optimization of (A)  $^1\text{H}$ - $^{13}\text{C}$  CP, and  $^1\text{H}$ - $^{15}\text{N}$  CP, and (B) simultaneous CP (SIM-CP). (C) Comparison of  $^{13}\text{C}$  and  $^{15}\text{N}$  sensitivity for CP and SIM-CP for a sample of U- $^{13}\text{C}$ ,  $^{15}\text{N}$  microcrystalline ubiquitin. The sensitivity is almost identical for CP and SIM-CP for the aliphatic region, whereas for the carbonyl region and  $^{15}\text{N}$  a minimal loss of sensitivity (less than 10%) is observed using SIM-CP sequence.

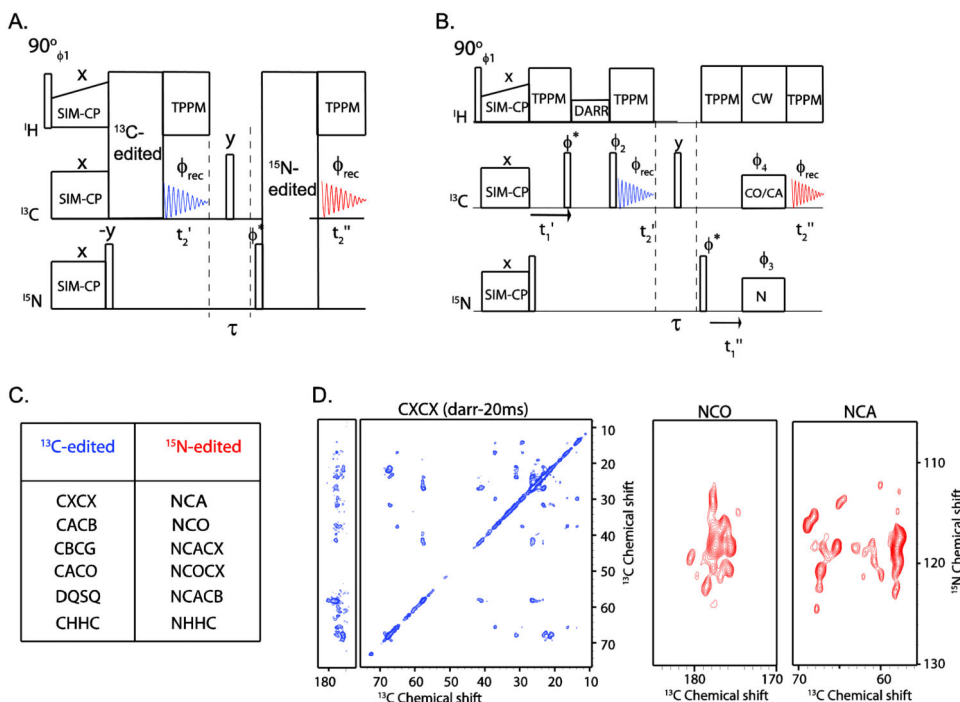


**Figure 2.**

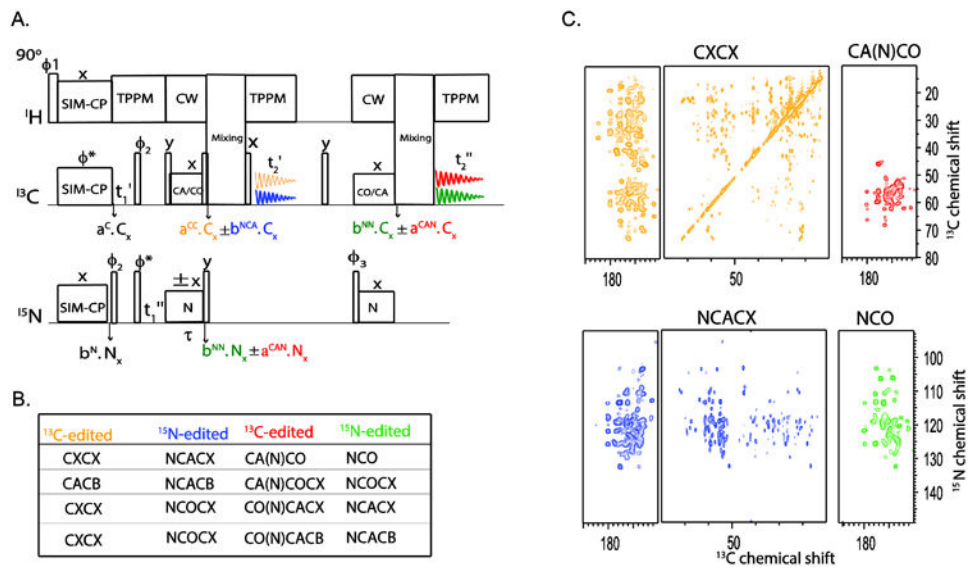
(A) Pulse sequence to measure the bidirectional polarization transfer from N to CA and vice-versa. The CA polarization is acquired in the first acquisition, whereas  $^{15}\text{N}$  polarization transferred to CO and detected during the second acquisition. (B) 1D spectra originating from the bidirectional polarization transfer on U- $^{13}\text{C}$ ,  $^{15}\text{N}$  crystalline ubiquitin using the pulse sequence shown in (A). The spectra were acquired with 32 scans and 3 ms contact periods for both NCA and NCO. The integrate intensity of carbonyl spectrum (red) is 48% of the CA spectrum (blue) due to two NC transfer periods.

**Figure 3.**

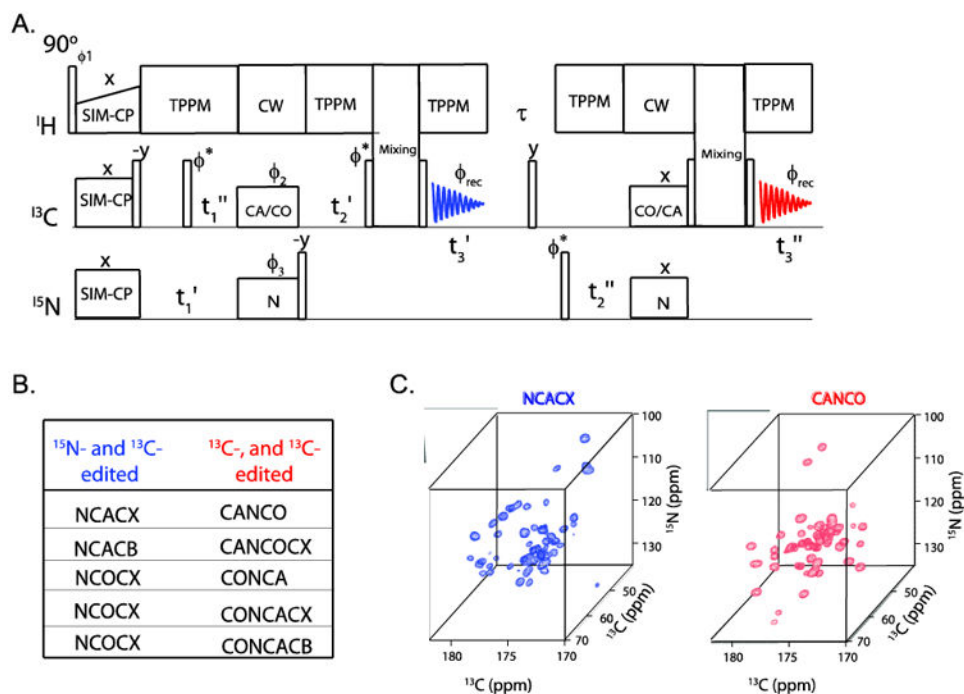
(A) Pulse sequence to measure the signal intensity of four polarization pathways resulting from NCA specific-CP. The  $^{15}\text{N}$  spin lock phase is set to  $+x$  and  $-x$  in alternate scans. The data are then decoded into four spectra using the procedure described within the text. (B) Experimental curves for the build-up of the four polarization pathways for a microcrystalline U- $^{13}\text{C}$ - $^{15}\text{N}$  ubiquitin sample and a DMPC reconstituted sarcosin sample. Normalized signal intensities were plotted as a function of specific-CP contact period  $\tau$ . (C) Representative 1D spectra obtained from pulse sequence (A) on a U- $^{13}\text{C}$ ,  $^{15}\text{N}$  microcrystalline ubiquitin sample shown in (B).



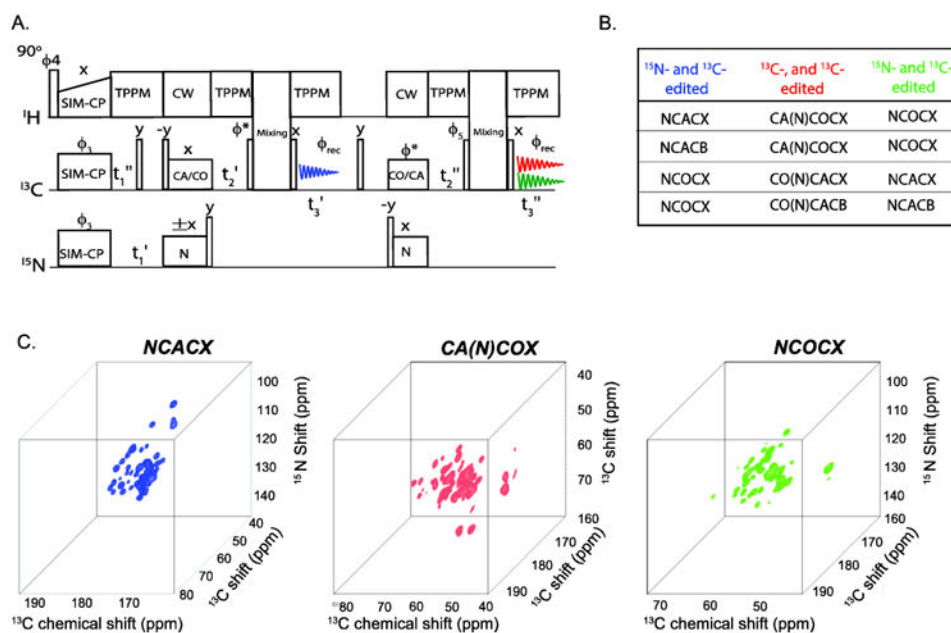
**Figure 4.** (B) A general schematic of 2D DUMAS for simultaneous acquisition of  $^{13}\text{C}$ - and  $^{15}\text{N}$ -edited experiments, as shown in (C). (B) An example of 2D DUMAS that combines a CXCX with an NCA or NCO experiment. (D) CXCX, NCA, and NCO spectra of sarcolipin obtained from 2D DUMAS in 10 hours of total experimental time. This experiment is divided into two parts, where CXCX and NCO are acquired in the first 6 hours using 16 scans, and another identical CXCX and NCA are acquired in the last 6 hours. The two CXCX data sets are then added before processing, whereas NCO and NCA are processed separately. The  $t_1$  evolution parameters are according to table 1, in which the number of increments for  $^{13}\text{C}$  evolution is 256, C is set to 8,  $^{13}\text{C}$  and  $^{15}\text{N}$   $t_1$  dwell times are 30 and 300  $\mu\text{s}$  respectively.

**Figure 5.**

(A) 2D MEIOSIS method for simultaneous acquisition of four 2D experiments that are listed in (B). An example of 2D MEIOSIS is method is demonstrated on U-<sup>13</sup>C,<sup>15</sup>N microcrystalline ubiquitin sample.

**Figure 6.**

A general pulse sequence diagram for 3D DUMAS for combining a pair of 3D experiments shown in (B). (C) Simultaneous acquisition of NCACX and CANCO on U-<sup>13</sup>C-<sup>15</sup>N ubiquitin using 3D DUMAS.

**Figure 7.**

Protocol of 3D MEIOSIS for simultaneous acquisition of three 3D experiments that are listed in (B), the first and second NC transfer are respectively set to NCA and NCO or vice versa. Two data sets are recorded with <sup>15</sup>N spin lock phase set to +x and -x. Sum of the two data sets of the second acquisition gives the NCC experiment (shown in green), whereas the difference of two data sets gives NCC (shown in blue) and C(N)CC (shown in red) associated with the first and second acquisitions, respectively. (C) Simultaneous acquisition of NCACX, CA(N)COCX and NCOCX on U-<sup>13</sup>C,<sup>15</sup>-N ubiquitin using 3D MEIOSIS shown in (A).

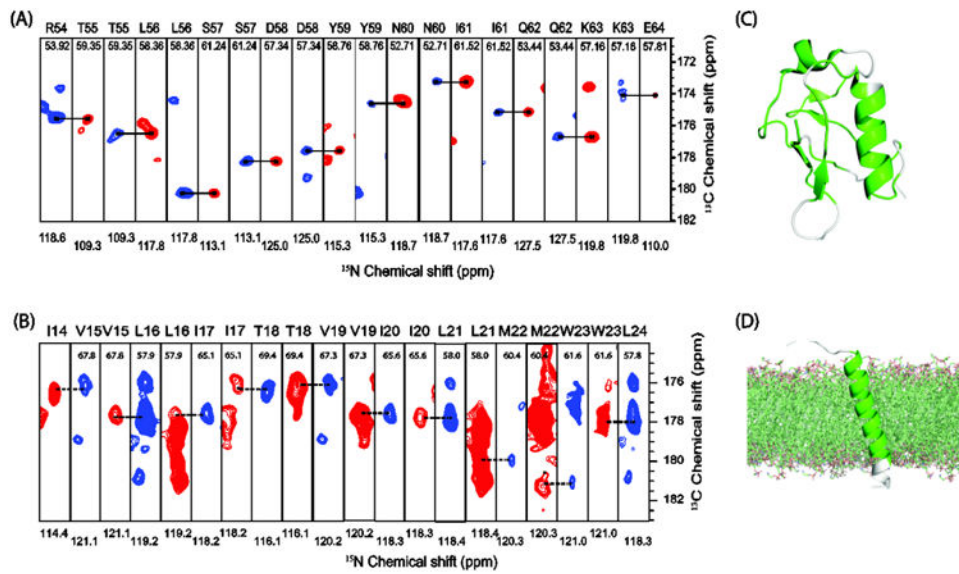


**Figure 8.** Sequential assignment of (A) ubiquitin, and (B) the membrane protein sarcolipin using the 3D DUMAS-NCACX-CANCO experiment shown in figure 6. Assigned residues from the 3D DUMAS experiment are highlighted in green on the secondary structure of ubiquitin (C), and sarcolipin (D).

**Table 1**

Criteria for  $t_1$  acquisition parameters for 2D DUMAS experiments. Here  $ni(t_1') \cdot ns(t_1') = ni(t_1'') \cdot ns(t_1'')$ , and 'C' is an integer.

Parameter	$t_1'$ ( $t_1$ evolution of an $^{13}\text{C}$ edited experiment)	$t_1''$ ( $t_1$ evolution of an $^{15}\text{N}$ edited experiment)
dw (dwell time)	dw ( $t_1'$ )	dw ( $t_1''$ )
ni (number of increments)	ni( $t_1'$ )	$ni(t_1'') = \left(\frac{1}{C}\right) \cdot ni(t_1')$
$t_{1\text{max}}$ (Maximum $t_1$ evolution)	$t_{1\text{max}}' = dw(t_1') \cdot ni(t_{1\text{max}}')$	$t_{1\text{max}}'' = dw(t_1'') \cdot ni(t_{1\text{max}}'')$
ns (number of scans)	ns( $t_1'$ )	$ns(t_1'') = C \cdot ns(t_1')$